Materials Science and Engineering A368 (2004) 56–70

MATERIALS SCIENCE & ENGINEERING A

www.elsevier.com/locate/msea

Comparison of different experimental techniques for determination of elastic properties of solids

M. Radovic*, E. Lara-Curzio, L. Riester

Metals and Ceramics Division, Oak Ridge National Laboratory, 1 Bethel Valley Road, PO Box 2008, Oak Ridge, TN 37831, USA

Received 28 June 2003; received in revised form 15 September 2003

Abstract

Four different experimental techniques, namely resonant ultrasound spectroscopy (RUS), impulse excitation (IE), nanoindentation (NI) and four-point bending (4PB) test were used to determine the Young's and shear moduli of 99.9% pure Al_2O_3, 7075 aluminum, 4140 steel and Pyrex glass. The results from the different tests are compared and statistically analyzed to determine the precision of each method and to estimate the significance of the differences among the four techniques. It was found that dynamic methods (RUS and IE) have superior precision and repeatability when compared to NI and 4PB for all four tested materials. It was also found that the differences between results of RUS and IE are not statistically significant, and that NI can be equally successfully used for determining Young's modulus of well-prepared, microstructurally homogenous and relatively hard materials. 4PB was found to have the lowest precision and repeatability among the four test methods.

Keywords: Elastic properties; Resonant ultrasound spectroscopy; Impulse excitation; Nanoindentation; Four-point bending

1. Introduction

The constitutive equations for a linear elastic solid provide a relationship between the stress and strain tensors according to

$$\sigma_{ij} = C_{ijkm}\varepsilon_{km} \quad (1)$$

where σ_{ij} and ε_{km} are the stress and strain tensors, respectively, and the tensor of elastic constants, C_{ijkm} has 81 components [1]. For an isotropic linear elastic solid the number of independent elastic constants is reduced to two. One of those constants involves dilatational deformation and the other one describes deformation by shear. These constants can also be expressed conveniently in terms of the so-called Young's modulus, E, and Shear modulus, G.

In general, individual crystal grains in materials are anisotropic, but polycrystalline solids comprised of randomly oriented grains exhibit isotropic (or quasi-isotropic) elastic behavior. The magnitude of the elastic constants of defect-free materials is only a function of the magnitude of the stiffness of the atomic bonds. In real polycrystalline materials, other factors, such as porosity, texture, concentration of impurities and alloying elements, intergranular phases, etc., may influence the magnitude of the elastic constants. Also, many materials exhibit anelastic behavior even at low loads [2], which can have an effect on the magnitude of measured moduli.

Considering the importance of elastic properties of materials for design and engineering applications, it is not surprising that a great number of experimental techniques have been developed to determine them. Broadly, those techniques can be classified into two groups [3]:

- Static techniques;
- Dynamic techniques.

Static methods are based on direct measurements of stresses and strains during mechanical tests (tensile, compressive, flexural, tensional, etc.), and Young's and Shear moduli are determined from the slope of the linear region of the stress–strain curve. Another popular static method for measurement of Young's modulus is nanoindentation (NI), especially when the amount or volume of material available is limited.

Dynamic techniques provide an advantage over static techniques because of ease of specimen preparation, wide

* Corresponding author. Tel.: +1-865-574-0034; fax: +1-865-574-0698.
E-mail address: radovicm@ornl.gov (M. Radovic).

0921-5093/$ – see front matter © 2003 Elsevier B.V. All rights reserved.
doi:10.1016/j.msea.2003.09.080

variety of specimen shapes and sizes, great precision, and measurement over a wide temperature range. Dynamic methods can be broadly classified into the two groups: resonance and pulse methods. In principle, resonant methods consist of setting a sample into mechanical (sonic and/or ultrasonic) vibration in one or more vibrational modes at one or more frequency at which the vibrational displacements are at a maximum (resonance). Samples can be excited to vibrate by drivers having continuously variable frequencies output [4] or by impact [5]. Vibrations of the sample are monitored by detecting transducers and analyzed in order to determine its characteristic frequencies. Knowing the vibrational mode, frequency, dimensions and mass of the samples it is possible to calculate the elastic constants of the material. Pulse techniques are generally based on measuring the transit time; that is the time spent for the ultrasonic pulse to travel through the specimen from the transmitting to the receiving transducer. By knowing the dimensions and density of the samples and the transit time for longitudinal and transversal ultrasonic waves it is possible to calculate Young's and Shear moduli of the material.

In this paper we report the room temperature elastic properties of four different materials determined by impulse excitation (IE), resonant ultrasound spectroscopy (RUS), nanoindentation and four-point bending (4PB) test. The results are compared and statistically analyzed in order to determine the precision of the measurement processes and to estimate the statistical significance of the differences among them. In this context, the precision is considered to be a closeness of agreement between test results obtained from the measurement process under the stipulated conditions [6,7].

2. Experimental procedure

Samples of different shape and size were prepared using Pyrex glass (manufacturer Corning[1], NY, supplier McMaster-Carr[1], GA), 7075 aluminum tempered T651 (McMaster-Carr[1], GA), 4140 steel cold finished according to ASTM A331 (McMaster-Carr[1], GA) and high purity Al_2O_3 (99.9% pure Al_2O_3, CoorsTek[1], CO). Table 1 lists the shape, dimensions, average roughness and parallelism of all tested samples. Dimensions and weight of all samples were measured with resolution of 0.001 mm and 0.0001 g, respectively. All aluminum samples were machined (cut by band saw or shaved by mill and additionally ground) from the same aluminum rod. The same procedure was used to machine all Steel samples, also from the same steel rod. Pyrex samples of different shape and size (Table 1) were cut using a diamond-impregnated wheel or core-drilled from two rolled glass sheets (original thickness of 3.28 and 6.53 mm). Al_2O_3 discs and bars were received from the supplier with final dimensions listed in Table 1 and no additional preparation was needed before testing. Average roughness and parallelism of the samples were measured using a Form Talysurf 120 Stylus Profiler (Taylor-Hobson[1], Leicester, UK) and a Legend IMS Coordinate measuring machine (EMD[1], Budd Lake, NJ), respectively. The surfaces of machined samples were additionally ground in order to obtain sharp edges, without chamfers and bevels that could have a significant effect on the determined magnitude of elastic constants [5,9]. Since the bulk density values of Al_2O_3 samples that were calculated form mass and dimensions of the samples varied significantly from sample to sample, the density of each Al_2O_3 sample was additionally measured by water immersion [8].

The elastic properties of all tested materials were determined using the experimental methods that are described in the following sections.

2.1. Four-point bending (4PB) test

Fig. 1 shows a schematic of the experimental setup for the four-point bending test [9]. The loading and supporting cylinders were free to rotate in order to relieve frictional constraints. Axial strain was measured a using 120 Ω, single unit strain gages (type FLA, Tokyo Sokki Kenkyujo Co.,[1] Tokyo, Japan) using quarter bridge 3-wire configuration. Strain gages were bonded on the tensile side of rectangular bars (Fig. 1) and their alignment was inspected using an optical microscope. The misalignment angle between the strain gage and the main axes of the samples never exceeded 1°. Strain (ε) and load were directly monitored during loading–unloading cycles using a data acquisition system (WBK512 and WBW16 Iotech[1], Cleveland, OH) at 100 Hz sampling rate. Samples were subjected to multiple loading–unloading cycles at a constant displacement rate of 1 mm/min. Maximum loads were always below the yield stress for 4140 steel and 7075 aluminum or below the bending strength of alumina and Pyrex glass. The magnitude of

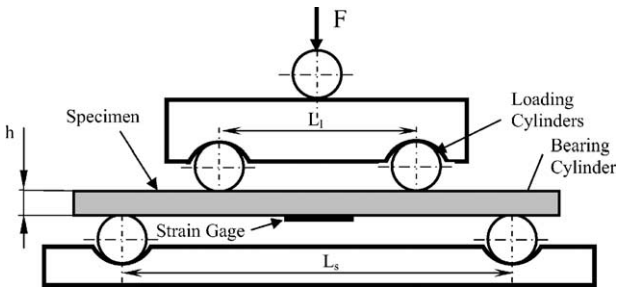

Fig. 1. Schematic of the setup for four-point bending test.

[1] Certain commercial equipment, instruments, or materials are identified in this paper in order to specify the experimental procedure adequately. Such identification is not intended to imply recommendation or endorsement by Oak Ridge National Laboratory, nor is it intended to imply that the materials or equipment identified are necessarily the best available for the purpose.

Table 1
Shape and dimensions of tested samples

Material	Sample	Shape[a]	Dimensions (mm)
Alumina	ALA-1	D	25.920 diameter × 1.983
	ALA-2	D	50.125 diameter × 2.390
	ALA-3	B	60.195 × 6.323 × 6.297
	ALA-4	B	60.198 × 6.327 × 6.298
	ALA-5	D	31.163 diameter × 2.422
	ALA-6	D	63.033 diameter × 2.989
		Average roughness R_a = 1.210 μm, parallelism = 0.0120 mm	
7075 Aluminum	A-1	D	25.410 diameter × 0.982
	A-2	D	25.423 diameter × 0.924
	A-3	D	25.430 diameter × 2.018
	A-4	D	25.455 diameter × 1.994
	A-5	D	25.453 diameter × 3.956
	A-6	D	25.398 diameter × 3.983
	A-7	B	59.973 × 4.979 × 6.961
	A-8	B	59.975 × 4.976 × 6.959
	A-9	P	24.978 × 17.071 × 2.003
	A-10	P	25.010 × 17.093 × 4.017
		Average roughness R_a = 0.421 μm, parallelism = 0.0066 mm	
4140 Steel	S-1	D	25.375 diameter × 0.993
	S-2	D	25.370 diameter × 0.992
	S-3	D	25.405 diameter × 1.999
	S-4	D	25.370 diameter × 2.002
	S-5	D	25.383 diameter × 1.999
	S-6	D	25.400 diameter × 3.991
	S-7	D	25.420 diameter × 3.991
	S-8	D	25.425 diameter × 3.987
	S-9	B	59.988 × 4.962 × 6.934
	S-10	B	59.940 × 4.969 × 6.949
	S-11	P	24.930 × 16.961 × 3.955
	S-12	P	24.972 × 16.965 × 1.975
		Average roughness R_a = 0.160 μm, parallelism = 0.0273 mm	
Pyrex glass	G1	D	57.045 diameter × 3.277
	G2	D	56.975 diameter × 6.524
	G3	D	28.105 diameter × 3.269
	G4	D	27.990 diameter × 6.534
	G5	P	25.438 × 28.610 × 3.267
	G6	P	25.453 × 28.908 × 6.524
	G7	B	60.068 × 5.033 × 6.530
		Average roughness R_a = 0.009 μm, parallelism = 0.0404 mm	

[a] Sample's shape: D 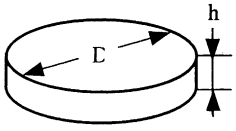

; Sample's shape: P 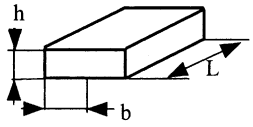

; Sample's shape: B—bar 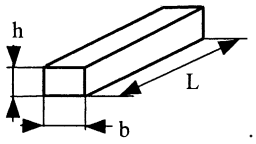

.

the stress on the tensile surface of the test specimen was calculated according to

$$\sigma = \frac{3}{2}\frac{F(L_s - L_l)}{bh^2} \quad (2)$$

where F, L_s, L_l, b and h are the measured load, support span, loading span, specimen width and specimen thickness, respectively (see Fig. 1). This method allowed the determination of Young's modulus of the tested samples from linear regression analysis of σ–ε curve. Selected but typical stress–strain curves obtained from four-point bend testing are presented in Fig. 2. Slopes of the loading and unloading curves were determined separately by linear regression. Correlation coefficients, R^2, close to 1 indicate the goodness of the fit of the results. In this case the slope is equal to the magnitude of the Young's modulus of the material.

2.2. Nanoindentation (NI)

Indentation at the nanometer scale with a Nanoindenter™ (Fig. 3) using a Berkovich diamond indenter is a widely used technique to determine mechanical properties of materials during indentation. The position of the indenter relative to

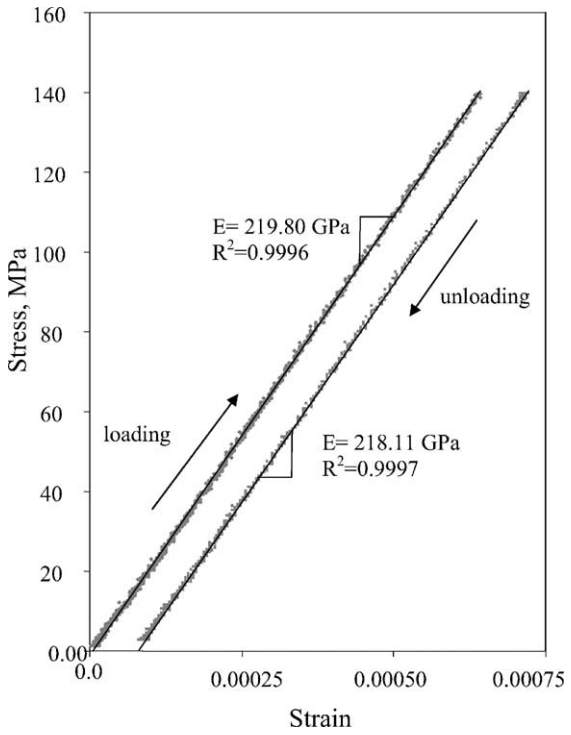

Fig. 2. Stress–strain curve for sample S-9 obtained from four-point bending test. The unloading curve is shifted to the right with respect to the loading curve for clarity.

the test surface of the specimen is constantly measured with a sensitive capacitance gage. The load applied to make the indent is monitored and recorded continuously as a function of displacement. Plastic and elastic components of displacement are separated either by continuous sensing of sample stiffness while force is being applied or held constant, or by

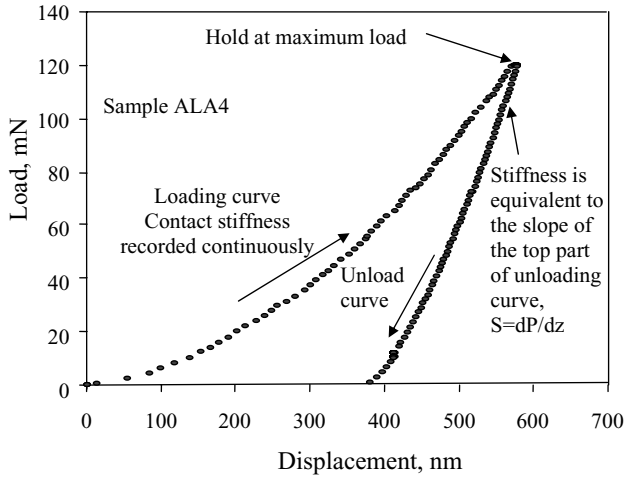

Fig. 4. Typical indentation load–displacement curve. Sample: ALA4. Contact stiffness is recorded continuously during the loading cycle and is equivalent to the slope of unloading curve.

calculating the stiffness which is equivalent to the slope of the top part of the unloading curve of the load/displacement cycle, as shown in Fig. 4. The relationship between contact or unloading stiffness and Young's modulus is defined in following equations:

$$S = \frac{2\beta}{\sqrt{\pi}}\sqrt{A}E_{\mathrm{r}} \tag{3}$$

where A is the contact area, E_{r} the reduced modulus and β an indenter geometry dependent constant (1.034 for the Berkovich indenter) [10], and

$$\frac{1}{E_{\mathrm{r}}} = \frac{1-\nu^2}{E} + \frac{1-\nu_0^2}{E_0} \tag{4}$$

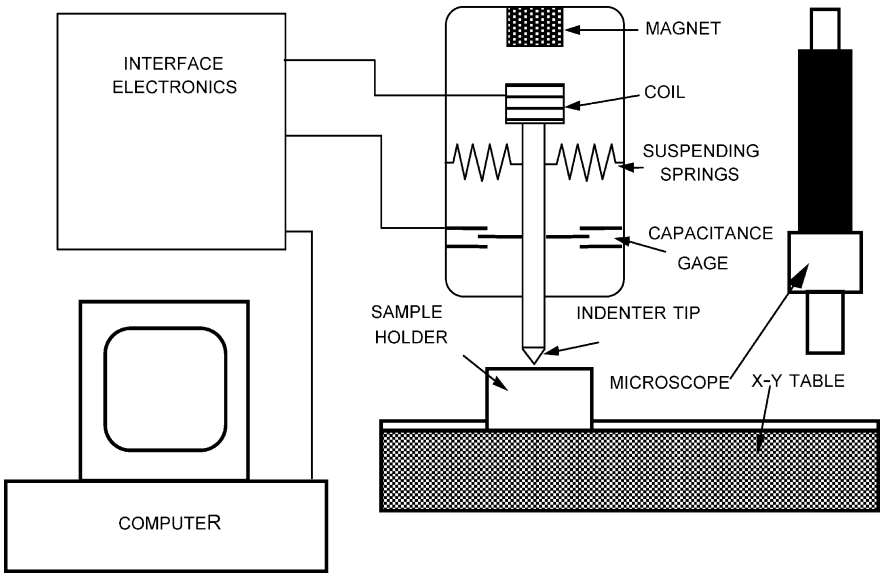

Fig. 3. Schematic of nanoindentation test.

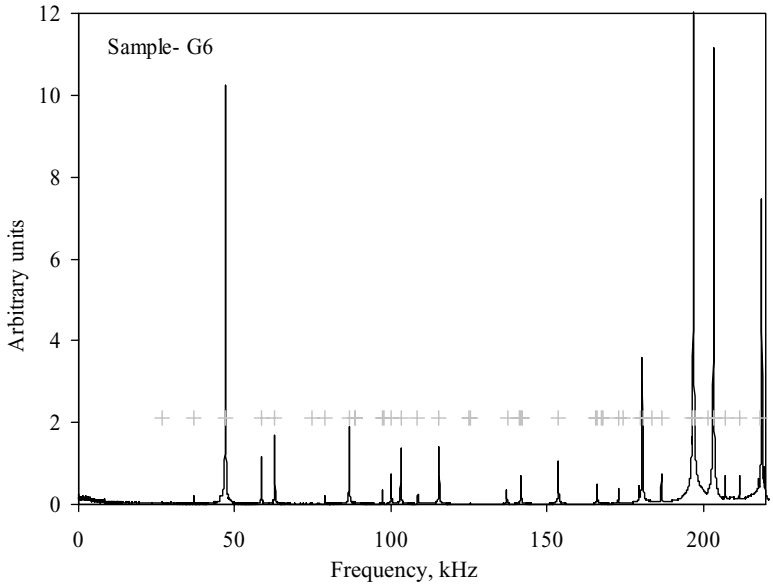

Fig. 5. Typical RUS spectra obtained for sample G6. Gray crosses indicate the peak frequencies obtained by fitting the measured spectrum.

where E and E_0 are the Young's modulus of the sample and the indenter, and ν and ν_0 the Poisson's ratio of the test material and the indenter, respectively.

Specimens for nanoindentation were mounted in epoxy and parallel, flat specimens with a mirror smooth surface were prepared following standard metallographic procedures to a final fine polishing step using 0.25 μm diamond paste. The Nanoindenter was calibrated for different indentation depths using fused silica as a calibration material. Experiments were conducted using the continuous stiffness method for either displacement or load control tests. This operating mode, whereby the indents tip is allowed to oscillate at constant amplitude, senses and records the contact stiffness of the material continuously during the indentation cycle. For 50, 100, 200 and 300 nm penetration depths, displacement control was chosen so that each loading segment would last 50 s (1 nm/s for 50 nm penetration depth, 2 nm/s for 100 nm penetration depth and so forth). Loading rates for load controlled experiments were 500 μN/s for maximum load of 20 mN, 1000 μN/s for maximum load of 40 mN, 2000 μN/s for 80 mN and 3000 μN/s for 120 mN, or 40 s in duration per loading segment. The slightly slower rate for shallow penetration depths permitted data points to be collected. After reaching selected maximum penetration depth or maximum load, a 15 s hold segment was used to allow the indenter to equilibrate for 10 s and to measure contact stiffness for the remaining 5 s. The indenter was then first unloaded for 80% at which point a longer, 60 s, hold segment was used to correct for any thermal drift that might have occurred during the indentation cycle. Contact stiffness from the loading and last part of the hold segments were compared to the slope of the unloading curve which represents the stiffness of the unloading segment (Fig. 4). Those values were found to be equivalent for the materials being evaluated. The average contact stiffness from the last five data points of the 15 s hold segment at maximum load was used to calculate the Young's modulus.

2.3. Resonant ultrasound spectroscopy (RUS)

Resonant ultrasound spectroscopy is a technique that can be used for determining elastic constants of solids. The technique is based on measuring the resonant spectrum (Fig. 5) of mechanical resonance for a sample of known geometry, dimensions and mass [11–13]. It is well known that the mechanical resonance frequencies of a freely suspended solid object are the special solutions to the equation of motion, which depend on density, elastic moduli and shape of the object. These solutions determine all possible frequencies at which such an object would "ring" if stuck [14].

A schematic of the experimental tripod setup for resonant ultrasound spectroscopy is shown in Fig. 6. The small discs or parallelepiped shaped specimens of tested materials were supported by three piezoelectric transducers. One transducer (transmitting transducer) is used to generate an elastic wave of constant amplitude and varying frequency, whereas the other two transducers are used to detect resonance. The spectrum obtained cannot be deconvoluted to deduce the elastic constants [11,12]. Instead, an approximate spectrum is calculated from the known sample dimensions, density and a set of "guessed" elastic constants. A multidimensional algorithm[2] to minimize root mean square (RMS) error between the measured and calculated resonant peaks enables the estimation of the elastic constants of the solid from the single frequency scan.

[2] Quasar International, Albuquerque, NM.

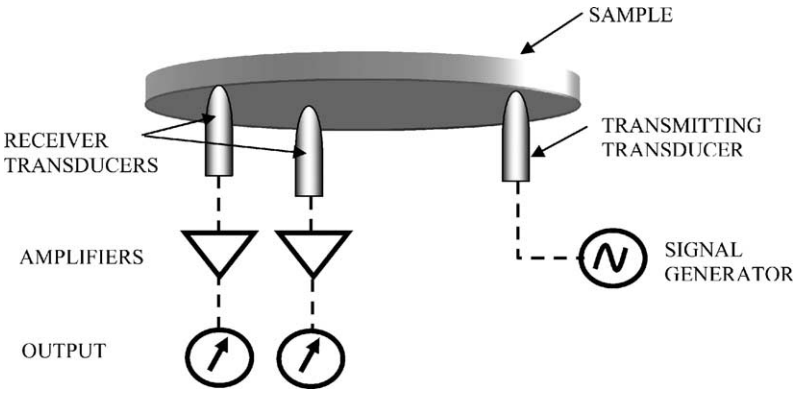

Fig. 6. Schematic of the tripod experimental setup for resonant ultrasound spectroscopy.

In this study, the first 40 resonant peaks were fitted for every tested sample assuming elastic isotropy (two independent elastic constants, Young's and Shear moduli). Two independent measurements were performed for each sample in the 0–200 kHz frequency range with 0.03 kHz frequency resolution. Goodness of fit was estimated using RMS error between measured and calculated peaks. Typically, the first 2–3 frequency peaks never fit well, especially in the case of very thin specimens (thickens to diameter ratio of <0.04) for which resonant spectra is shifted towards lower frequencies. Those frequencies were excluded form the fitting process.

2.4. Impulse excitation (IE) technique

Impulse excitation (IE) allows the determination of dynamic Young's and Shear moduli from the resonant frequencies of a mechanically excited sample [15]. According to this test procedure a disc-shaped specimen is supported by a foam material on its nodal lines (Fig. 7) and then excited by a light mechanical impulse. The impulse tool used for this study consisted of an Al_2O_3 ball (1/8 in. diameter) attached to the end of the thin elastic rod. A microphone, located in the vicinity of the sample is used to transmit sound vibrations to the signal processing unit. The fundamental resonance frequencies, in both flexural and torsional mode, are identified, which in turn can be used to calculate values of Young's and Shear moduli using the following equation [5]:

$$E_{1,2} = \frac{37.6991 f_{1,2}^2 D^2 m(1-\nu)}{K_{1,2}^2 t^3} \quad (5)$$

where D, m, and t are the diameter, mass and thickness of the sample, respectively. Poisson's ratio, ν is determined according to ASTM C1259 as a function of $2t/D$ and f_2/f_1. $K_{1,2}$ are the first and second natural geometric factors listed in ASTM C1259 as a function of μ and $2t/D$. $E_{1,2}$ are Young's moduli values calculated from the first (f_1) and second (f_2) natural resonant frequencies. Shear modulus, G, was determined according to the following equation:

$$G = \frac{E}{[2(1-\nu)]} \quad (6)$$

In this study, the commercially-available Buzz-o-sonic[1] (BuzMac Software, Glendale, WI) program was used to determine the fundamental frequencies and calculate the elastic moduli of the samples.

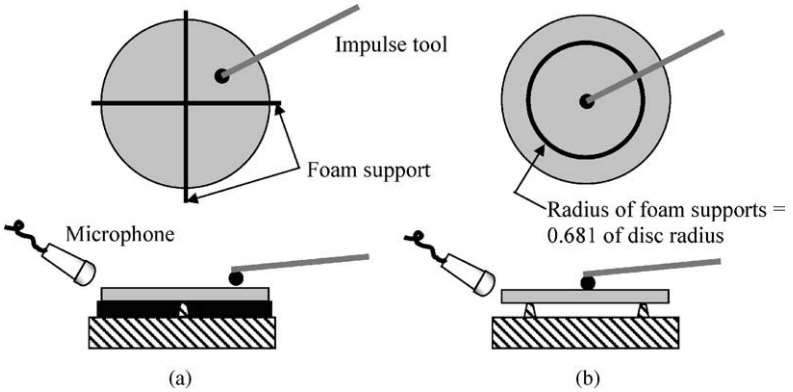

Fig. 7. Schematic of support setup for impulse excitation technique: (a) torsional mode of vibration and (b) flexural mode of vibration.

Table 2
Results of RUS for Pyrex glass

Sample	n	E				G				RMS (%)
		$\bar{X}$ (GPa)	S (GPa)	CV (%)	T (GPa)	$\bar{X}$ (GPa)	S (GPa)	CV (%)	T (GPa)	
G1	2	61.23	0.20	0.34	1.79	25.61	0.06	0.25	0.57	0.24
G2	2	61.92	0.06	0.09	0.54	25.93	0.04	0.15	0.36	0.20
G3	2	61.31	0.05	0.09	0.45	25.56	0.05	0.19	0.45	0.29
G4	2	61.67	0.01	0.01	0.09	25.81	0.01	0.05	0.13	0.14
Discs	8	61.53	0.32	0.52	0.27	25.75	0.02	0.08	0.17	
G5	2	60.13	0.03	0.05	0.27	25.61	0.02	0.08	0.18	0.33
G6	2	61.85	0.02	0.04	0.18	25.82	0.07	0.27	0.63	0.20
Plates	4	61.58	0.37	0.61	0.59	25.81	0.03	0.14	0.30	
All samples	12	61.55	0.31	0.49	0.19	25.77	0.14	0.55	0.09	

Table 3
Results of IE for Pyrex glass

Sample	n	E				G			
		$\bar{X}$ (GPa)	S (GPa)	CV (%)	T (GPa)	$\bar{X}$ (GPa)	S (GPa)	CV (%)	T (GPa)
G1	10	61.10	0.01	0.02	0.01	25.39	0.00	0.05	0.00
G2	10	61.48	0.03	0.05	0.02	25.56	0.02	0.11	0.01
All samples	20	61.29	0.2	0.32	0.09	25.47	0.09	0.78	0.04

3. Results

Results of Young's and Shear moduli measurements are lists in Tables 2–17. Every table contains:

- $\bar{X}$: mean value calculated from n measurements;
- S: standard deviation calculated as $S = \sqrt{\sum_{i=1}^{n}(X_i - \bar{X})^2/(n-1)}$;
- CV: coefficient of variation calculated as: CV (%) $= 100S/\bar{X}$;
- T: boundaries of 95% confidence interval estimate for the mean calculated as: $T = t_{n-1}S/\sqrt{n}$ where t_{n-1} is the critical value of the t-distribution (Student's distribution) with $n-1$ degrees of freedom for area of 2.5 % in upper tail;
- n: number of repetitions.

3.1. Pyrex glass

Results of elastic properties measurements for Pyrex glass are listed in Tables 2–5. Elastic moduli values determined by RUS, IE and NI are very close to each other. Also, relatively low values of standard deviation, coefficient of variation, and 95% confidence interval for all tested samples indicate that the values determined are very narrowly distributed. In the case of NI, the coefficients of variation for each sample are slightly higher than those calculated from RUS and IE results. Analysis of variance (ANOVA) [16,17] at the 95% confidence level shows that there are no statistically significant differences among mean values determined from RUS, NI and IE. Young's modulus values from 4PB (Table 3) are typically higher than those determined by RUS, NI and IE and they have the broadest distribution (CV = 1.392%) compared to the other techniques. ANOVA analysis (with 95% confidence) confirmed statistically significant differences between mean values measured using 4PB and other techniques. It is worth noting that Young's moduli of Pyrex glass determined in this study are in good agreement with the published values that ranges from 60 to 64 GPa [18].

Table 4
Results of 4PB for Pyrex glass

Sample	n	E			
		$\bar{X}$ (GPa)	S (GPa)	CV (%)	T (GPa)
G7-loading	3	63.31	1.16	1.84	1.08
G7-unloading	3	63.30	0.49	0.77	0.51
G7	6	63.30	0.88	1.39	0.53

3.2. 7075 Aluminum

Elastic properties of the aluminum samples determined by different techniques are listed in Tables 6–9 and they are close to the published values of $E = 72$ GPa and $G = 26.8$ GPa for 7075 aluminum [19]. In this case, the mean values of the elastic constants determined by RUS and IE are almost identical, although the distribution of results obtained by IE is broader than the distribution of the results obtained by RUS. The magnitude of the coefficient of variation for each sample evaluated by IE is relatively low and does not exceed 0.25%, indicating the high reproducibility of the measurement. An analysis of variance showed that the mean values determined by RUS and IE are equivalent at the 95% confidence level. The magnitude of Young's modulus

Table 5
Results of NI for Pyrex glass, sample G7

Displacement (nm)	Maximum load (mN)	n	E			
			$\bar{X}$ (GPa)	S (GPa)	CV (%)	T (GPa)
51.20	0.35	9	62.33	0.60	0.96	0.46
101.80	1.20	9	61.53	0.76	1.23	0.57
204.12	4.43	9	61.44	0.62	1.00	0.47
306.16	9.64	9	61.01	0.33	0.53	0.25
443.02	19.98	5	61.46	0.60	0.96	0.73
632.46	39.97	5	61.49	0.71	1.16	0.99
901.32	79.96	5	60.79	0.46	0.75	0.57
1106.61	119.95	5	61.208	0.50	0.82	0.62
All samples	56	61.45	0.71	1.16	0.19	

Table 6
Results of RUS for aluminum

Sample	n	E				G				RMS (%)
		$\bar{X}$ (GPa)	S (GPa)	CV (%)	T (GPa)	$\bar{X}$ (GPa)	S (GPa)	CV (%)	T (GPa)	
A1	2	70.67	0.10	0.14	0.90	25.91	0.47	1.83	4.26	0.48
A2	2	71.37	0.25	0.35	2.24	26.20	0.07	0.27	0.63	0.77
A3	2	71.46	0.19	0.27	1.73	26.55	0.03	0.10	0.25	0.37
A4	2	71.01	0.08	0.12	0.76	26.44	0.04	0.16	0.38	0.29
A5	2	71.51	0.04	0.06	0.37	26.63	0.01	0.03	0.06	0.15
A6	2	71.69	0.02	0.03	0.18	26.68	0.01	0.05	0.13	0.13
Discs	12	71.28	0.37	0.53	0.24	26.40	0.31	1.19	0.20	
A9	2	71.99	0.07	0.10	0.63	26.83	0.01	0.03	0.07	0.46
A10	2	71.77	0.01	0.01	0.05	26.72	0.09	0.32	0.77	0.18
Plates	4	71.88	0.13	0.18	0.21	26.77	0.06	0.22	0.09	
All samples	16	71.43	0.42	0.59	0.22	26.49	0.32	1.20	0.17	

Table 7
Results of IE for aluminum

Sample	n	E				G			
		$\bar{X}$ (GPa)	S (GPa)	CV (%)	T (GPa)	$\bar{X}$ (GPa)	S (GPa)	CV (%)	T (GPa)
A1	10	70.06	0.17	0.25	0.12	26.10	0.09	0.36	0.07
A2	10	72.87	0.08	0.11	0.06	26.78	0.05	0.17	0.03
All samples	20	71.47	1.45	2.03	0.68	26.44	0.35	1.34	0.17

determined by 4PB is slightly higher that those determined by RUS and IE, while values obtained by NI are significantly higher (9.7% higher that those determined by RUS). Not surprisingly, an analysis of variance confirmed that a statistically significant difference exists between mean values determined by 4PB and NI and those determined by RUS and IE, at the 95% confidence level. Not only are the mean values of moduli obtained from 4PB and NI higher than those from RUS and IE, but their distribution is much broader (higher variation and broader 95% confidence boundaries).

3.3. 4140 Steel

Tables 10–13 list elastic moduli values obtained from the evaluation of 4140 steel samples and they are close to the

Table 8
Results of 4PB for aluminum

Sample	n	E			
		$\bar{X}$ (GPa)	S (GPa)	CV (%)	T (GPa)
A7-loading	3	77.65	0.26	0.33	0.65
A7-unloading	3	74.13	1.17	1.57	2.89
A7	6	75.89	2.07	2.73	2.17
A8-loading	3	73.72	0.44	0.59	1.08
A8-unloading	3	70.40	0.20	0.28	0.49
A8	6	72.06	1.84	2.56	1.93
All loading	6	75.68	2.18	2.88	2.28
All unloading	6	72.27	2.18	3.01	2.28
All samples	12	72.27	2.07	2.87	1.32

Table 9
Results of NI for aluminum, sample A2

Displacement (nm)	Maximum load (mN)	n	E			
			$\bar{X}$ (GPa)	S (GPa)	CV (%)	T (GPa)
52.08	0.16	6	77.38	2.81	3.63	2.95
103.79	0.53	6	77.52	1.39	1.80	1.46
206.05	1.85	6	79.13	0.56	0.70	0.58
309.47	4.02	6	80.63	1.35	1.67	1.41
310.33	4.01	6	78.85	1.96	2.49	2.06
718.05	19.97	6	78.93	1.06	1.35	1.12
1018.63	39.95	6	78.16	1.47	1.88	1.54
1452.76	79.94	6	74.02	1.30	1.76	1.36
1751.76	119.92	6	80.18	1.79	2.23	1.87
All samples	54	78.31	1.941	2.48	0.53	

Table 10
Results of RUS for steel

Sample	n	E				G				RMS (%)
		$\bar{X}$ (GPa)	S (GPa)	CV (%)	T (GPa)	$\bar{X}$ (GPa)	S (GPa)	CV (%)	T (GPa)	
S1	2	209.20	0.06	0.03	0.57	81.23	0.03	0.04	0.32	0.29
S2	2	209.13	0.12	0.06	1.07	81.21	0.12	0.15	1.08	0.34
S3	2	210.36	0.07	0.03	0.60	81.76	0.02	0.03	0.19	0.09
S4	2	210.59	0.07	0.03	0.64	81.81	0.01	0.02	0.13	0.17
S5	2	210.25	0.03	0.02	0.31	81.76	0.00	0.00	0.00	0.12
S6	2	211.39	0.05	0.02	0.46	82.11	0.02	0.03	0.19	0.17
S7	2	211.63	0.02	0.01	0.14	82.27	0.13	0.15	1.14	0.22
S8	2	211.57	0.11	0.05	1.01	82.14	0.03	0.03	0.25	0.14
Discs	12	210.57	0.96	0.45	0.51	81.78	0.39	0.47	0.20	
S11	2	211.44	0.10	0.05	0.91	82.24	0.16	0.19	1.40	0.282
S12	2	210.52	0.16	0.07	1.40	81.89	0.11	0.13	0.95	0.29
Plates	4	210.98	0.54	0.25	0.86	82.07	0.23	0.28	0.36	
All samples	16	210.61	0.90	0.43	0.42	81.84	0.37	0.45	0.17	

published values of $E = 205$ GPa and $G = 80$ GPa for 4140 steel [19]. In this case, elastic constants determined by RUS, NI and IE are almost identical. Also, the distribution of the results is relatively narrow with the highest coefficient of variation of 1.259% in the case of IE. An analysis of variance showed that there is no significant statistical difference, at the 95% confidence level, among values measured using those three techniques. Results from NI have much broader distribution (CV = 6.09%) than RUS data. Standard deviation, coefficient of variation and 95% confidence intervals for low penetration depths are considerably higher than those obtained at high penetration depths (Table 13). The magnitude of Young's modulus obtained from 4PB is considerably higher than those measured by other techniques, which was confirmed by an analysis of variance at the 95% confidence level.

3.4. Al_2O_3

The values of Young's and shear moduli of Al_2O_3 samples determined by different techniques are listed in Tables 14–16. In Fig. 8, these results are presented as a

Table 11
Results of IE for steel

Sample	n	E (GPa)				G (GPa)			
		$\bar{X}$ (GPa)	S (GPa)	CV (%)	T (GPa)	$\bar{X}$ (GPa)	S (GPa)	CV (%)	T (GPa)
S1	10	205.85	0.21	0.10	0.15	78.26	0.30	0.38	0.21
S2	10	205.16	0.04	0.02	0.03	77.82	0.01	0.02	0.01
S12	10	210.90	0.29	0.14	0.21	84.95	0.10	0.11	0.07
All samples	30	207.30	2.61	1.26	0.97	80.34	3.32	4.14	1.24

Table 12
Results of 4PB for steel, sample S4

Sample	n	E			
		$\bar{X}$ (GPa)	S (GPa)	CV (%)	T (GPa)
S9-loading	3	220.44	0.73	0.33	1.82
S9-unloading	3	218.58	0.15	0.07	0.38
S9	6	219.51	1.13	0.51	1.18
S10-loading	3	219.08	0.35	0.16	0.86
S10-unloading	3	217.31	0.52	0.24	1.30
S10	6	217.94	0.77	0.36	0.81
All loading	6	219.76	0.90	0.75	0.95
All unloading	6	217.94	0.77	0.36	0.81
All samples	12	218.73	1.23	0.56	0.78

Table 13
Results of NI for steel, sample S4

Displacement (nm)	Maximum load (mN)	n	E			
			$\bar{X}$ (GPa)	S (GPa)	CV (%)	T (GPa)
52.43	0.81	6	216.01	12.89	5.97	13.53
103.69	1.40	6	223.63	14.12	6.32	14.82
207.00	0.84	6	222.22	11.38	5.12	11.95
309.91	1.43	6	219.41	5.28	2.41	5.54
312.10	2.56	6	219.99	3.54	1.61	3.72
464.39	9.70	6	213.54	6.45	3.02	6.77
667.43	8.45	6	206.70	3.69	1.79	2.88
962.36	9.12	6	187.55	7.28	3.88	3.88
1172.77	14.09	6	208.14	2.903	1.39	2.23
All samples		57	212.76	12.96	6.09	3.44

Table 14
Results of RUS for Al_2O_3

Sample	n	E				G				RMS (%)
		$\bar{X}$ (GPa)	S (GPa)	CV (%)	T (GPa)	$\bar{X}$ (GPa)	S (GPa)	CV (%)	T (GPa)	
ALA1	2	365.27	0.12	0.03	0.30	81.23	0.03	0.04	0.32	0.50
ALA2	2	385.27	0.06	0.02	0.15	81.21	0.12	0.15	1.08	0.42
ALA5	2	369.10	0.25	0.07	0.62	81.76	0.02	0.03	0.19	0.36
ALA6	2	346.04	0.23	0.07	0.61	81.81	0.01	0.01	0.13	0.40
All samples	8	366.42	14.92	4.07	12.47	148.50	5.65	3.80	5.22	

Table 15
Results of IE for Al_2O_3

Sample	#	E				G			
		$\bar{X}$ (GPa)	S (GPa)	CV (%)	T (GPa)	$\bar{X}$ (GPa)	S (GPa)	CV (%)	T (GPa)
ALA2	16	387.24	0.32	0.08	0.17	154.98	0.21	0.14	0.11
ALA6	16	338.56	0.32	0.09	0.17	135.65	0.23	0.17	0.12
All samples	32	362.90	24.73	6.82	8.92	145.32	9.82	6.76	3.54

Table 16
Results of 4PB for Al_2O_3

Sample	#	E			
		$\bar{X}$ (GPa)	S (GPa)	CV (%)	T (GPa)
ALA3-loading	3	381.59	7.32	1.92	18.19
ALA3-unloading	3	387.02	0.91	0.23	2.26
ALA3	6	384.31	5.54	1.44	5.81
ALA4-loading	3	403.55	1.30	0.32	3.23
ALA4-unloading	3	395.79	1.75	0.44	4.36
ALA4	6	399.67	4.47	1.12	4.69
All loading	6	392.57	12.92	3.29	13.56
All unloading	6	391.41	4.96	1.27	5.21
All samples	12	391.99	9.35	2.38	5.91

Table 17
Results of NI for Al_2O_3

ALA1			ALA2			ALA4			ALA5			ALA6		
d (nm)	E (GPa)		d (nm)	E (GPa)		d (nm)	E (GPa)		d (nm)	E (GPa)		d (nm)	E (GPa)	
	$\bar{X}$	S		$\bar{X}$	S		$\bar{X}$	S		$\bar{X}$	S		$\bar{X}$	S
51.4	417.12	21.36	51.3	435.86	12.20	51.7	415.85	34.35	53.38	412.01	13.20	51.1	374.76	93.74
103.1	405.92	24.56	102.8	431.63	5.32	103.4	409.14	40.62	105.8	416.88	9.84	103.2	372.36	83.45
201.0	423.33	5.63	198.2	418.52	4.92	202.2	424.42	30.62	201.8	404.97	8.33	200.0	427.11	11.27
206.5	408.08	12.77	206.4	421.52	8.37	207.9	413.53	32.57	209.7	395.43	18.88	206.8	395.53	55.85
291.5	407.51	13.89	292.1	395.91	7.84	286.8	423.89	11.03	302.2	376.38	24.83	307.5	388.07	57.29
308.8	395.00	12.57	307.6	407.66	7.10	309.9	411.14	25.66	312.6	373.11	8.920	308.3	405.11	30.62
310.2	406.08	19.21	311.9	405.94	6.77	312.0	411.08	14.57	313.2	379.71	19.11	310.3	406.85	16.24
431.5	378.11	7.31	430.6	373.91	14.44	427.7	390.71	13.23	434.5	357.23	12.19	441.2	382.64	20.83
536.7	373.58	10.67	521.6	407.57	6.65	551.4	382.00	10.25	530.7	387.14	14.5	533.3	396.17	21.04
All	398.81	17.77		407.83	17.5		408.24	14.87		386.36	19.00		396.73	16.75

d: displacement or penetration depth.

function of porosity. Analysis of the results obtained from the evaluation of different Al_2O_3 samples revealed a much broader distribution than for Pyrex glass, aluminum and steel. On the other hand, coefficients of variation calculated from the results obtained for every single Al_2O_3 sample by RUS and IE, are not significantly higher than those obtained for Pyrex, steel and aluminum, and do not exceed 0.17%. Thus, the relatively high coefficients of variation for all tested samples cannot be related to the lower reproducibility of the experimental results, but rather to the differences in the "intrinsic" elastic properties of the samples evaluated. This is not surprising if we consider that the porosity of Al_2O_3 samples varies from sample to sample (Table 18).

Young's and Shear moduli determined by RUS and IE techniques are plotted in Fig. 8 as a function of the measured porosity of tested samples. The magnitude of both E and G decreases as the porosity increases. Two empirical relations, namely Linear [20] and Exponential [21] were fitted to experimental moduli determined by RUS and the fitting parameters are listed in Table 19. Relatively high coefficients of correlation indicate that all data can be well described with both the linear and exponential relations.

The predicted values for Young's and Shear moduli (E_0 and G_0, respectively) of fully dense Al_2O_3 obtained with both fitting models are close to each other, as shown in Table 19.

The magnitude of Young's moduli values determined by NI and 4PB are significantly higher that those obtained by RUS and IE (Fig. 8). Also, the distribution of results is significantly broader than for Pyrex, aluminum and steel, especially in the case of NI.

Table 18
Porosity of tested alumina samples determined by water immersion

Sample	Porosity (%)
ALA1	2.95
ALA2	1.57
ALA3	2.36
ALA4	4.27
ALA5	2.71
ALA6	2.71

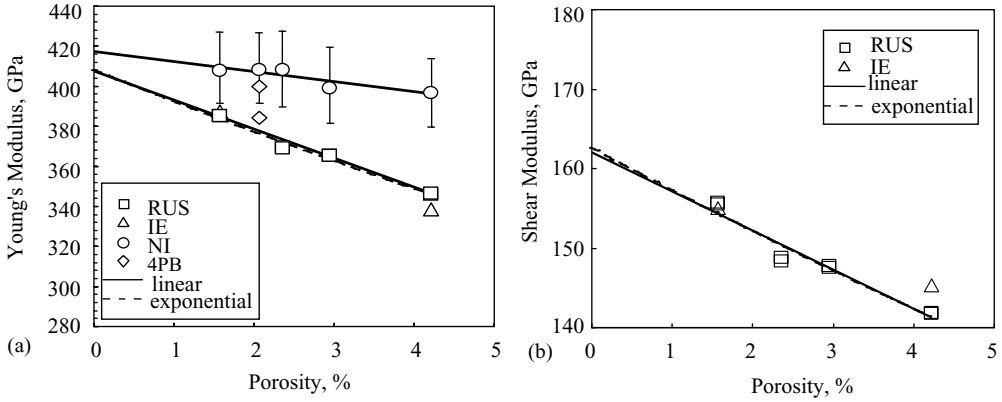

Fig. 8. Determined (a) Young's modulus and (b) shear modulus as a function of porosity for alumina.

Table 19
Results of fitting RUS data using linear and exponential relationships between moduli and porosity

Linear	$E = E_0(1 - bp)$	$E_0 = 410.97 \pm 3.09$	$b = 0.038 \pm 0.003$	$R = 0.98$
	$G = G_0(1 - bp)$	$E_0 = 162.25 \pm 1.46$	$b = 0.030 \pm 0.003$	$R = 0.97$
Exponential	$E = E_0 \exp(-bp)$	$E_0 = 407.60 \pm 2.60$	$b = 0.038 \pm 0.002$	$R = 0.99$
	$G = G_0 \exp(-bp)$	$E_0 = 164.01 \pm 1.66$	$b = 0.0352 \pm 0.003$	$R = 0.97$

p is porosity (%), E_0 and G_0 are the Young's and shear moduli of fully dense material, respectively, and b and R the characteristic constant and correlation coefficient, respectively.

4. Discussion

The variation of Young's and shear moduli determined by different experimental techniques clearly shows high precision of the dynamic techniques, namely resonant ultrasound spectroscopy and impulse excitation. This observation is in good agreement with previously published studies [22]. Also, reported results indicate that for Pyrex glass and steel, high precision can be achieved using nanoindentation. In all cases, it was found that the results obtained from four-point bend testing are significantly higher than those determined by RUS, IE and NI.

The lowest variability of the results measured for each separate sample (repeatability) is achieved using RUS and IE where the coefficients of variation for each sample never exceed 0.5%. These values are in good agreement with the coefficients of variations obtained from interlaboratory round-robin tests on precision of IE [5]. The results of the round-robin study (reported in ASTM C1259 [5]) showed that the coefficients of variations for individual laboratories ranged from 0.001 to 1% for two tested materials. Also, relatively low values of overall coefficients of variation for all tested samples indicate high precision in all cases, except for Al_2O_3. In that case, the porosity of the samples varies significantly from sample to sample and thus the results obtained for different samples cannot be compared to calculate a general coefficient of variation.

The overall coefficient of variation calculated for results obtained from IE is slightly higher in the case of Aluminum than those calculated for Pyrex and steel. The lower Young's modulus for sample A1 determined using both RUS and IE results in higher values of standard deviation and coefficient of variation in the case of IE where only two samples were evaluated (Table 7), than in the case of RUS where six samples were evaluated (Table 6). Also, in all cases analysis of variance carried out at the 95% confidence level shows that there is no significant statistical difference between mean values of Young's and shear moduli determined by RUS and IE. Even in the case of Al_2O_3 samples, values measured for each sample by IE and RUS are close to each other (Fig. 8).

It is worth noting that an analysis of variance did not reveal statistically significant differences at the 95% confidence level between RUS results obtained with disc-shaped and plate-shaped test specimens. This is important because the frequencies of the large number of vibrational modes (so called degenerative modes) overlap in resonant spectra of symmetrical samples (like discs) [11] reducing the number of peaks in the acquired spectra. According to our results this does not have a significant influence on the precision of the measurements for symmetrical samples, at least when a relatively large number of peaks (40 in this study) is used in the fitting process.

The high precision of dynamic methods allows the precise determination of the elastic constants of samples with different porosity (1.58–4.22 vol.%). Analysis of the effect of porosity on elastic properties of tested Al_2O_3 samples (Fig. 8, Table 19) using Linear and Exponential models predict a value of the Young's modulus for fully dense Al_2O_3 that is close to previously published data (400–414 GPa) [23,24].

Since the determination of elastic properties using dynamic methods, RUS and IE, is sensitive to the dimensions

Table 20
Minimum and maximum variation of results obtained by IE and RUS as a function of variation in measured dimensions of the samples

Sample	Thickness, CV (%)	Diameter, CV (%)	IE				RUS			
			E		*G*		*E*		*G*	
			CV (%)		CV (%)		CV (%)		CV (%)	
			Minimum	Maximum	Minimum	Maximum	Minimum	Maximum	Minimum	Maximum
S1	0.12	0.04	−0.38	0.29	−0.58	0.29	−0.34	0.34	−0.24	0.30
S2	0.19	0.78	−0.68	0.77	−0.68	0.77	−0.037	0.59	−0.28	0.46
A1	2.65	0.04	−8.70	7.82	−8.70	7.82	−7.30	5.41	−9.03	5.72
A2	2.95	0.78	−9.37	8.37	−9.38	8.43	−7.8	6.23	−0.3	4.49
G1	0.12	0.08	−0.48	0.52	−0.51	0.50	−0.50	0.30	−0.27	0.19
G2	0.02	0.06	−0.16	0.23	−0.14	0.24	−0.18	0.40	−0.07	0.19
ALA2	1.21	0.10	−3.86	5.31	−3.87	3.69	−2.45	3.17	−2.8	1.8
ALA6	1.34	0.06	−3.99	4.14	−4.04	4.56	−3.47	3.14	−3.08	2.40

of the test specimens [11], the effect of variability in sample dimensions on the magnitude of the elastic constants, determined from IE and RUS, was analyzed using the minimum (X_{min}) and maximum (X_{max}) dimensions calculated as: $X_{min} = \bar{X} - \text{S.D.}$ and $X_{max} = \bar{X} + \text{S.D.}$, where $\bar{X}$ and S.D. are mean values (from Table 1) and standard deviations, respectively, for diameter or thickness of the sample. Coefficients of variation for Young's and shear moduli obtained using the minimum and maximum dimensions are calculated using elastic constants obtained for mean values of measured dimensions (from Tables 2, 3, 6, 7, 10, 11, 14 and 15) as a reference value. Minimum and maximum values of those coefficients of variation are listed in Table 20 as a function of coefficient of variation for measured dimensions (diameter and thickness) of the samples. The results presented in Table 20 demonstrate the high sensitivity of both RUS and IE to uncertainty in the magnitude of the specimen dimension. Small variations in dimensions (CV up to 0.2%) result in small variations for elastic constants (from −0.68 to 0.77%) that are comparable to those listed in Tables 2, 3, 6, 7, 10, 11, 14 and 15. In the case of higher variations in measured dimensions (CV up to 2.95%) elastic coefficients differ from those calculated for mean values of measured dimensions by as much as ±9.38%. The results listed in Table 20 also demonstrate that values of elastic constants determined from RUS and IE for disk-shaped samples are more sensitive to variations in the thickness than to variations in the diameter of the sample. Results listed in Table 20 also suggest that differences in sensitivity to the uncertainty in the magnitude of the specimen dimension between RUS and IE are practically insignificant.

Besides the high precision, the most important advantage of RUS and IE is that for isotropic materials both yield the independent elastic constants, c_{11} and c_{44}. Although RUS and IE are very precise methods, the high sensitivity to variations in dimensions of the samples is one of the major disadvantages for their application for determination of elastic constants. In order to get precise results, both techniques require well-prepared samples without surface or bulk defects, and with parallel, flat and smooth surfaces. When making the decision on which of those two dynamic techniques should be used to determinate elastic constants it has to taken into account that RUS is a more complicated technique than IE, and it requires an experienced operator, initial knowledge of the approximate values of elastic constant and a significant amount of time for analysis of the experimental results. On the other hand, RUS allows the determination of elastic constants of a small samples (below 1 mm [11]) and elastically anisotropic test specimens. Furthermore, RUS offers the possibility of determining elastic constant at cryogenic or elevated temperatures.

While there is no statistically significant difference among the values of Young's moduli determined by NI, RUS and IE for Pyrex glass and steel, they are significantly different in the case of aluminum and Al_2O_3. Even in the case of good agreement between the RUS, IE and NI results, the coefficients of variation for NI are higher than those from RUS and IE suggesting a broader distribution of measured values. This is not surprising, because in NI the elastic response of the small amount of material surrounding the indentation is measured, and thus local microstructural differences between different indentations do have an effect on measured values.

A significantly higher value of Young's modulus for 7075 aluminum was obtained from NI compared to values determined by RUS and IE. Even for 4041 steel samples, the magnitude of Young's modulus determined by NI is slightly higher than those determined by RUS and IE, although an analysis of variance did not show statistically significant differences between mean values determined by those three techniques at the 95% confidence level.

Young's Moduli values obtained from NI are significantly higher than those measured by RUS and IE for each alumina sample (Fig. 8). Also, the difference between results obtained by RUS and IE and those from NI, increases as porosity of the test specimens increases. Fitting the NI results from Table 7 using a linear model and extrapolating to zero porosity results in Young's modulus of fully dense material $E_0 = 417$ GPa, which is only 1.7% higher than that listed in Table 19. Also, NI results for Al_2O_3 exhibit more scatter than those obtained for other tested materials. This can be attributed to the significant differences in microstructure of

porous Al_2O_3 samples at the micro level. Differences between determined values from indent to indent reflect the variation of the elastic response of the material around the indentation area. If an indent is far from a pore, the elastic response of the porous material will be similar to that of a fully dense material, while if an indent is too close to a pore, the elastic response will be affected by the presence of the pore.

The results obtained in this study indicate that high precision can be achieved in the determination of Young's modulus through nanoindentation for well-prepared, micostructurally homogenous and relatively hard materials. One of the major disadvantages of nanoindentation is its high sensitivity to microstructural inhomogeneities in the sample and on the finish of the surface that is indented. Also, in order to calculate the Young's modulus from obtained results one has to know or guess the value of Poisson's ratio for the material being evaluated. Although, assumed value does not have significant effect on the calculated value of Young's modulus, this could be considered as a disadvantage of nanoindentation technique. On the other hand, nanoindentation allows the determination of Young's modulus using very small volumes of material, which could not be evaluated by RUS and IE (e.g. thin films). However, it has to be emphasized that nanoindentation requires specialized equipment and an experienced operator.

In general, it was found that the variability of results obtained from four-point bending is significantly higher than those associated with RUS, NI and IE, except in the case of Al_2O_3. This is true for both the variability of results obtained with the same sample (low repeatability), and variability of results among various samples of the same material. According to the results of an analysis of variance, the values of Young's modulus measured by 4PB are in all cases significantly different, at the 95% confidence level, from those obtained by the three other techniques investigated. The magnitude of the elastic moduli determined by 4PB in this study were found to be always higher than those obtained from RUS, IE and NI. The differences between elastic moduli determined by static and dynamic methods have been studied by others [22,25] and it is believed that uncertainties in the value of the static elastic modulus and strain gage readings may be of the order of several percents which could account for the slightly greater moduli determined by 4PB [25].

5. Conclusions

The Young's and Shear moduli of Pyrex glass, Al_2O_3, 7075 aluminum and 4140 steel were determined at room temperature by resonant ultrasound spectroscopy and impulse excitation Technique. Also, Young's moduli of all four materials were obtained at room temperature using nanoindentation and four-point bend testing. An analysis of the results suggests the following points:

- Dynamic methods (RUS and IE) have superior precision, for all tested samples, than NI and 4PB, and that there is no significant difference between results obtained by RUS and IE.
- Nanoindentation can be successfully used for determination of Young's modulus of well-prepared and micostructurally homogenous materials. In that case, values and variability of results obtained by NI results are close to those obtained by RUS and IE. However, it was found that the variability of results obtained by nanoindentation of porous samples was very large, due to lack of microstructural homogeneity in the region surrounding the indents.
- The precision of four-point bend testing is lower than those of the other three techniques. Furthermore, the magnitude of Young's modulus determined by 4PB not only differs significantly from those obtained by RUS, IE and in some cases by NI, but also the coefficient of variation is higher compared to those obtained from RUS, NI and IE.

Acknowledgements

This research work was sponsored by the US Department of Energy, Office of Fossil Energy, SECA Core Technology Program at ORNL under Contract DE-AC05-00OR22725 with UT-Battelle, LLC. The authors are grateful for the support of NETL program managers Wayne Surdoval and Donald Collins. The authors are indebted to Richard Counts of ORNL for stimulating discussions and valuable suggestions regarding the statistical analysis of the results and to Arvid Pasto of ORNL for reviewing the manuscript. Help provided by Randy Parten of ORNL during the specimen's preparation is also greatly appreciated.

References

[1] N.E. Dowling, Mechanical Behavior of Materials, Prentice Hall, Upper Side River, NJ, 1998.
[2] R. Schaller, G. Fantozzi, G. Gremaud (Ed.), Mechanical Spectroscopy Q-1 2001: With Applications to Materials Science (Materials Science Forum, vols. 366–368), Trans Tech Publications, Ltd., Uetikon, Zurich, 2001.
[3] P.E. Armstrong, in: R.F. Bunshan (Ed.), Measurement of Mechanical Properties, Techniques of Metals Research, vol. V (Part 2), Wiley, New York, 1971, pp.103.
[4] ASTM Standard C1198-96.
[5] ASTM Standard C1259-98.
[6] ASTM Standard E177-90a.
[7] ASTM Standard E456-02.
[8] ASTM Standard C373-88.
[9] ASTM Standard C1161-02.
[10] W.C. Oliver, G.M. Pharr, J. Mater. Res. 7 (6) (1992) 1564.
[11] A. Migliori, J.L. Sarrao, Resonant Ultrasound Spectroscopy: Applications to Physics, Materials Measurements and Nondestructive Evaluation, Wiley, New York, 1997.
[12] A. Migliori, J.L. Sarrao, W.M. Visscher, et al., Phys. B 183 (1993) 1.
[13] R.B. Schwarz, J.F. Vuorinen, J. Alloys Compd. 310 (2000) 243.
[14] W.M. Visscher, A. Migliori, T.M. Bell, R.A. Reinert, J. Acoust. Soc. Am. 90 (4) (1991) 2154.

[15] R.W. Walpole, R.H. Mayers, Probability and Statistics for Engineers and Scientists, second ed., Macmillan, New York, 1972.
[16] R.L. Scheaffer, J.T. McClave, Statistics for Engineers, Duxbury Press, Boston, 1982.
[17] H.M. Wadsworth, Handbook of Statistical Methods for Engineers and Scientists, Mc-Graw-Hill, New York, 1990.
[18] M. Bauccio (Ed.), ASM Engineering Materials Reference Book, ASM International, Materials Park, OH, 1994.
[19] J.R. Davis (Ed.), Metals Handbook, ASM International, Materials Park, OH, 1990.
[20] E.A. Dean, J.A. Lopez, J. Am. Ceram. Soc. 66 (5) (1983) 366.
[21] R.M. Springs, J. Am. Ceram. Soc. 54 (9) (1962) 452.
[22] H. Ledbetter, Mater. Sci. Eng. A165 (1993) L9.
[23] K.K. Phani, S.K. Niyogi, J. Mater. Sci. 22 (1987) 257.
[24] J.C. Wang, J. Mater. Sci. 19 (1984) 809.
[25] G. Quinn, J. Swab, J. Am. Ceram. Soc. 83 (2) (2000) 317.